Laser Transfer of Metal Contacts and Dopants for Silicon Solar Cells

---

A Thesis

Presented to

the faculty of the School of Engineering and Applied Science

University of Virginia

---

in partial fulfillment

of the requirements for the degree

Master of Science

by

Longteng Wang

May

2014

APPROVAL SHEET

The thesis

is submitted in partial fulfillment of the requirements

for the degree of

Master of Science

Longteng Wang

AUTHOR

The thesis has been read and approved by the examining committee:

Mool C. Gupta

Advisor

Lloyd R. Harriott

Arthur W. Lichtenberger

Accepted for the School of Engineering and Applied Science:

Dean, School of Engineering and Applied Science

May

2014

ACKNOWLEDGEMENTS

I wish to express my sincere thanks to Professor Mool C. Gupta, who has been a devoted mentor to both my research and study. His advising methodology, insightful guidance and constant support have made this thesis possible. I have been deeply grateful to the opportunity given by him to join this group and the research on laser processing for silicon solar cells. His encouragement has strongly motivated me through the venture of research.

I also want to thank Dr. David E. Carlson for collaborating with our group and providing with insightful analysis and technical advice. I'm deeply encouraged by his broad view of solar research community. I'm honored to have the opportunity of working with him.

I extend my gratitude to Professor Harriott and Professor Lichtenberger for taking their valuable time serving in my thesis committee and providing valuable input.

Sincere thanks also go to Keye Sun who has been a patient senior lab mate helping me with lab activities. I also acknowledge the help from Dr. Vikram Iyengar, Dr. Tyson Baldridge, Dr. Jiguang Li, Dr. Yang Shen and Christian Rothenbach.

My deep gratitude and sincere appreciation go to my wife Man Xu and my parents, who have supported me so much along the way. My endeavor was only possible with their persistent encouragement and mental companion.

This work is financially supported by NASA Langley Professor Program and NSF I/UCRC award.

Abstract

Crystalline silicon has been the primary raw material in the industrial manufacturing of solar cells. Silicon Photovoltaics (PV) technologies have been advancing rapidly towards higher efficiency, cost reduction and simplification of fabrication processes. Traditional processes, including emitter and metal contacts formation, have been largely relying on high-temperature process. In this dissertation, we explored alternative processes using a laser-based approach for reduction of cost due to low temperature processing.

A pulsed ytterbium fiber laser has been used for metal contacts formation and doping process for silicon solar cell fabrication using laser transfer. Both front and rear metallization were achieved through laser induced forward transferring. The crystalline silicon solar cell based on all-laser-transferred contacts (ALTC) was fabricated on chemically textured p-type Cz silicon wafers with a simple cell structure of full-area emitter. An initial conversion efficiency of over 15% was achieved. To demonstrate the laser transfer of dopants, a phosphorous dopant was laser transferred through the dielectric passivation and antireflection layer followed by metallization using electroplating. The resultant silicon solar cell has line-shaped junctions formed by laser transferring process and showed current density as high as 34.5 mA/cm^2 without any surface texturing. Both optical and electrical characterizations were carried out to study the laser transfer of metal contacts and dopants. Simulations were performed using PC1D and PC2D to better understand the limitations and future improvements. The ALTC and laser transfer of dopants demonstrate the advantage of laser processing in simplifying the

solar cell fabrication process also replaces the high-temperature furnace with room-temperature process.

Table of contents

LIST OF FIGURES

LIST OF TABLES

LIST OF SYMBOLS

d	Line-shape junction spacing
E	Laser energy density
N	Number of overlapping laser pulses
I_{sc}	Short circuit current
J_{sc}	Short circuit current density
V_{oc}	Open circuit voltage
FF	Fill factor
R_s	Series resistance
R_p	Shunt resistance
τ	Bulk minority carrier lifetime
S_n	Surface recombination velocity
λ	Wavelength
EQE	External Quantum Efficiency
PECVD	Plasma Enhanced Chemical Vapor Deposition
Al-BSF	Aluminum Back Surface Field
PV	Photovoltaics
PERC	Passivated Emitter and Rear Cell
IBC	Interdigitated Back Contact
LFC	Laser Fired Contacts
ALTC	All Laser Transferred Contacts
SOD	Spin-on Dopant
SEM	Scanning Electron Microscope
EDX	Energy-dispersive X-ray Spectroscopy
LBIC	Laser Beam Induced Current

CHAPTER 1: INTRODUCTION AND MOTIVATION

1.1 Silicon Solar Cell and Fabrication

A silicon solar cell operates based on the principles of Photovoltaics. Following the absorption of sun light inside silicon wafer, photo-generated electron-hole pairs are created. Then the electric field separates the electrons and holes and they are finally collected by the respective metal contacts.

Surface textures are generally introduced on the front surface of silicon wafer to enhance light absorption. The majority of silicon solar cells are based on p-type silicon wafers. Therefore, n-type emitter is created on the front side generally by phosphorus dopants diffusion. A dielectric layer of SiN_x (or other materials such as SiO_2 or a-Si) is necessary on top of the emitter for the purpose of both anti-reflection coating and passivation. The metal contacts for collecting electrons and holes are formed on front and rear sides respectively. Silver is normally used for the front side metal contacts. The metal pattern is fingers with crossed busbar. Aluminum is used for the rear metallization and it covers the whole surface.

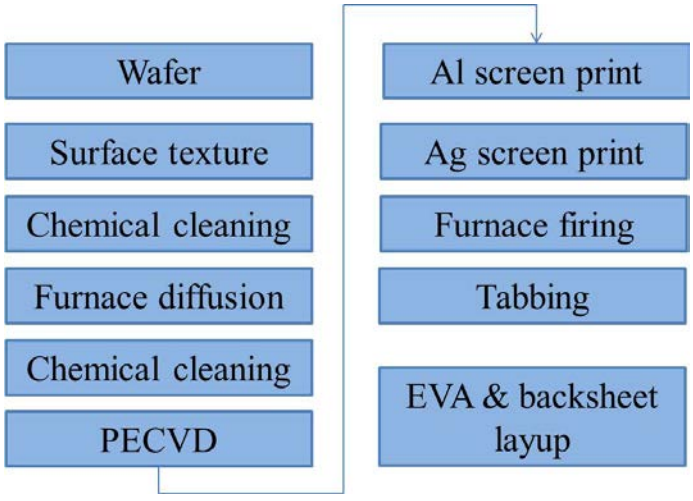

Figure 1. Fabrication steps for silicon solar cells

The research in silicon solar cells is advancing rapidly towards advanced cell structures with constant improvements in lowering manufacturing cost, increasing cell efficiency and ramping up production volume [1]. The majority of current silicon solar cell manufacturing has been based on p-type wafer based cell structure with blanket n-type emitter on the front and full area Al contact on the rear side.

Major steps of traditional process flow for fabricating silicon solar cells are shown in figure 1. The Si wafers are first chemically textured on the front surface to introduce roughness that will reduce surface reflection and enhances light absorption. Rigorous cleaning is then performed in the wet bench to remove any surface metal and organic contaminations. The wafers are then inserted into the furnace for diffusion of dopants to form emitters. This diffusion is normally carried out at elevated temperature of more than 800℃ in the dopant gas ambient to form emitters. This is followed by removal of surface doping residual. A thin layer of SiN_x, or stack of SiN_x/SiO_x, is deposited on the front surface by PECVD to serve as both anti-reflection and passivation dielectrics. Rear and front side contacts are formed by screen printing of aluminum and silver respectively followed by belt furnace firing at elevated temperature and controlled belt speed. The firing step also creates back surface field (Al-BSF) for p-type silicon solar cells. A working solar cell is produced at this step. To connect the individual solar cells for the solar module, additional silver printing on the Al side is needed for the soldering of copper ribbon in the tabbing step. After tabbing using copper ribbon, certain numbers of solar cells are electrically connected to rated output voltage and current. The final step of mounting backsheet and EVA lamination helps protecting from moisture and dust for enhanced endurance in the outdoor environment.

1.2 Metallization and Doping Techniques

Metallization is a key step that determines the final device performance and it also counts for a major part of the fabrication cost. Ever since its introduction to PV industry in 1975, screen printing has been thoroughly studied and has become the most widely adopted technique for metallization in production lines [2- 4]. However, this technique suffers from several drawbacks. First of all, most screen-printed contacts have low aspect ratios with line width of around 100 μm [5]. This results in shadowing losses that reduce the solar cell output current. Finer line widths are possible with screen printing, but this requires more complicated design of wires, mesh and emulsion layers [6]. Secondly, a high temperature (~700-800 °C) firing process is required for screen printing metallization. The temperature profile has a significant consequence on the contact resistance and must be optimized [7, 8]. Thirdly, metal particles are generally mixed with glass in the printing paste, and the glass frit chemistry and metal particle sizes have to be tailored carefully in order to achieve a low contact resistance [9]. In addition, there is significant mechanical pressure during screen printing process which could result in wafer breakage. All these disadvantages will become more evident as the PV industry moves into low-cost production with thinner silicon wafers. Therefore, alternative methods for metallization need to be explored. Plating has recently regained the interests of researchers for solar cell metallization, and both electro and electroless plating methods have been developed for copper, nickel and other metals [10]. These methods were either to thicken seed contact layers or to directly form electrical contacts after performing a patterning step [11].

Traditionally, the emitter doping is achieved through high temperature diffusion in a gas ambient, such as phosphoryl chloride ($POCl_3$), for n type emitter formation. This has been extensively studied and utilized in industrial production. This process generally involves elevated temperature over 800℃ with controlled gas flow and temperature ramping profiles. The silicon wafers have to be immersed in the furnace chamber, and as a result the whole wafer is heated. This could result in significant degradation of bulk minority carrier lifetime especially for the industrial boron-doped crystalline silicon wafers [12]. The other drawbacks include high infrastructure cost of the diffusion furnace system which also requires significant maintenance. Besides gas phase doping, the liquid phase doping in the form of spin-on glass has also been extensively studied [13,14]. However, this again normally requires a furnace diffusion process that heats the whole wafer.

1.3 Objectives of Research

The objectives of this research are to demonstrate and investigate the laser transferring process of metal contacts and dopants as an alternative to the traditional metallization and diffusion processes for silicon solar cell fabrications. This laser transferring process shows the advantage of simplified fabrication process and only requires localized heating of silicon surface without affecting the whole wafer bulk. This process is realized at room temperature and requires smaller footprint of equipment.

The experimental conditions of laser transferring metal contacts and dopants were studied to understand the effects of laser parameters. Optical, electrical and morphology characterizations were carried out. A silicon solar cell based on all-laser-transferred contacts (ALTC) was fabricated for the first time. Silicon solar cells fabricated based on laser transferred dopants was also demonstrated to propose an all-laser-transfer process. Simulations were also performed to understand the limitations of current process and future improvements.

1.4 Thesis Outline

Chapter 1 briefly introduces the traditional fabrication process of silicon solar cells and the associated drawbacks of traditional diffusion and metallization processes. The overview is based on traditional cell structure with uniform full area emitter on the front and full area Al-BSF on the rear side.

Laser transfer of metal contacts is discussed in chapter 2. The fabrication process of all-laser-transferred-contacts (ALTC) is demonstrated for the first time on crystalline silicon wafers. Optical and electrical characterizations are made to understand this process. Device results based on laser transferred contacts are discussed with simulations to indicate future improvements. Laser transfer of dopants is discussed in chapter 3. The experimental process is described. Electrical characterization using LBIC and cell performance is investigated. PC2D simulation is performed to discuss the junction geometry and predict future improvements. Conclusions and future work of the laser transfer process for silicon solar cells are summarized in chapter 4.

Chapter 5 introduces additional research utilizing laser welding process and Al foil for the rear contact formation of silicon solar cells. Morphology and electrical contact resistivity of laser welded Al foil to silicon are characterized. Device performance is also measured.

CHAPTER 2: LASER TRANSFER OF METAL CONTACTS

2.1 Introduction

Laser processing has been investigated for solar cell fabrication and is drawing a great deal of attention [15-18]. Laser processing is contact-less and self-masking by its nature and therefore has a strong potential of simplifying the solar cell manufacturing process. In addition, laser only heats the treated sample locally without affecting the whole bulk material. This feature of laser processing is significantly valuable in preserving the bulk minority carrier lifetime especially for the boron-doped crystalline silicon wafers (Cz and Fz), which can be strongly affected by high temperature processing [12, 19]. Many papers have been published about laser processing techniques for metallization of silicon solar cells. Laser can directly produce silicon-metal contacts through processes such as laser-fired contacts and laser micro-sintering of metal particles [20, 21]. In other research, lasers have been used to indirectly assist metallization by selectively ablating dielectric layers for subsequent plating or metal evaporation [22, 23]. Some laser processing metallization techniques have been considered for industrial production such as the BP Solar laser-grooved buried contact cells [24]. However, there are drawbacks associated with these techniques. Laser micro-sintering requires additional cleaning steps afterwards to remove the un-sintered particles. The applications of laser-fired contacts are generally limited to aluminum on the un-illuminated cell side. Laser ablation of dielectrics relies on other metallization techniques, and thus requires additional processing steps. Therefore, alternative laser processing methods need to be explored.

Laser transferring of metals for contacting silicon solar cells is based on the technique of Laser Induced Forward Transfer (LIFT) or originally called Laser Writing after its invention in 1969 [25]. It is independent of the type of metal to be transferred, and various metals have been transferred for various applications [26-29]. Recently, nickel was laser transferred for front-side metallization of silicon solar cells [30, 31]. A transparent glass substrate was coated with evaporated nickel and then placed on top of a silicon substrate with an anti-reflection coating (ARC). A pulsed green (λ = 532 nm) laser beam with a pulse width of 10 ns was focused onto the glass surface. The local heating and subsequent interfacial boiling transferred nickel from the glass substrate through the ARC and then formed the nickel-silicon contact. Nickel and copper plating were performed afterwards to thicken the metal contacts. Contact resistivities lower than 1 mΩ-cm^2 after plating and conversion efficiencies as high as 17.4% were achieved with a selective emitter structure. However, the dark current of the processed device was high and the transferring was required to align with a selectively doped emitter. This increases the complexity of processing, and misalignment could occur.

In this work, all the contacts for the front and rear sides of the silicon solar cell were achieved by the laser transferring process. Prior to laser transfer, the silicon substrate is processed with a full-area emitter and dielectric layers passivating both the front and rear surfaces. Since the cell structure is simple with a single-step diffused uniform emitter, no aligning is needed for the laser transfer of metal. The front and rear electrode patterns are defined by the laser scanning. Overlapping laser pulses transfer and fire the metals through the ARC into the silicon in one single pass of laser scanning. Titanium is laser-transferred for the front contact seed layer, which is thickened by a

subsequent electro-plating process. Aluminum is laser-transferred through the passivation layer for contacting the rear side, which is finally coated with evaporated aluminum. It is interesting to point out that this All-Laser-Transferred Contacts (ALTC) process is compatible with the high-efficiency PERC structure [32], but the fabrication process would be simplified by laser transferring. In the current work, it is believed that an Al back surface field is formed during the laser transferring process as the laser power is high enough to drive the diffusion of aluminum into silicon.

2.2 Experimental

P-type boron-doped (ρ=1 Ω-cm; thickness=300 microns) mono-crystalline <100> silicon wafers (Cz) were used in this work. Wafers were first cleaned in acetone and methanol to remove any organic contaminants during handling, and then surface oxides were etched by dipping in diluted HF. Texturing of the front surface was carried out using TMAH solutions at 80℃ for 30 minutes[33]. Solar cell processing before laser transferring metallization followed the lab procedures outlined in reference [34]. The wafers were first cleaned in the Piranha solution at 85℃ for 10 minutes for removal of organic and metallic contaminants. Then the wafers were placed on the spinner with spin-on phosphorous dopant at 3500 rpm for 30 seconds. This resulted in a coating of spin-on glass of about 200 nm in thickness on the textured surface. The coated wafers were then inserted into the tube furnace for drive-in diffusion at 900℃ for about 15 minutes in an N_2 (80%) and O_2 (20%) ambient. This created a junction depth of about 400 nm in thickness and sheet resistance of about 40 Ω/sq. The thermal oxidation was carried out in the tube furnace at 850℃ for about 20 minutes to produce passivation layer of about 15

nm. Then a SiN_x layer of about 60 nm was deposited on the front side by PECVD. This SiN_x layer serves as both ARC and passivation in combination with the thermal oxide [35]. For cells based on All-Laser-Transferred Contacts, another layer of SiN_x was deposited on the rear side with a thickness of about 120 nm. This has the function of passivation as well as a back reflector according to reference [36]. Thus, prior to laser transferring of metal, an emitter was formed on front surface of the silicon wafer, and both sides were passivated. For the control device, the front metallization was achieved through photolithography and e-beam evaporation. A Ti/Pd/Ag stack of 50 nm/50 nm/1000 nm was used and further thickened by electro-plating of Ag to around 3 μm. A rear aluminum contact and back surface field were formed using Ferro 53-038 paste. After coating with this paste, the wafer was first soft baked at 200 °C and then inserted into a tube furnace at 800 °C for 5 minutes. Annealing in forming gas (95% Ar, 5% H_2) environment at 400℃ for about 2 minutes was carried out after cell fabrication.

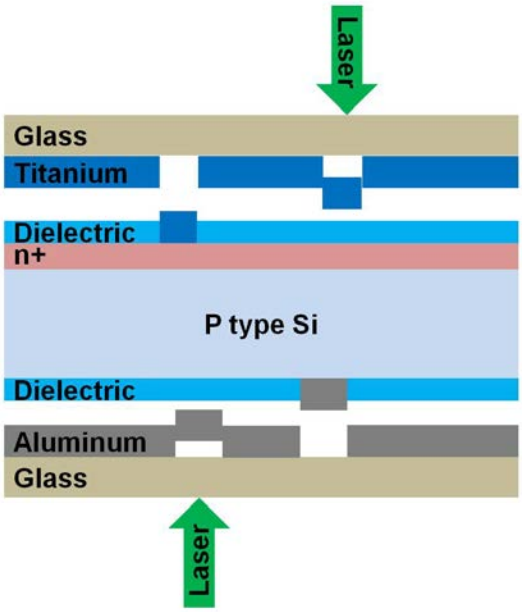

Figure 2. Schematic of laser transferring process for metal contact formation on both front and rear sides of a silicon solar cell.

Figure 2 illustrates the ALTC process for a silicon solar cell. Soda lime glass slides (refractive index = 1.52 at λ = 546 nm, thickness = 1.2 mm) were coated with evaporated titanium of thickness of 500 nm or with aluminum of the same thickness and then brought in contact with solar cell processed silicon wafer. A gap between glass and silicon wafer is shown in figure 2 for clarification. In practice, the metal-coated glass is placed directly on top of the silicon substrate. However, it should be pointed out that a gap could be introduced for non-contact processing purposes. A pulsed ytterbium fiber laser (IPG Photonics: YLP-G-10) with pulse width of 1 ns and wavelength of 532 nm was used. The pulse energy was about 16 µJ at 100% setting with a repetition rate of 20 kHz. A laser beam with a Gaussian profile first enters a galvanometer scanhead and is then focused by an f-theta objective lens on the working plane with a focal spot of about 20 µm in diameter. The working plane can be moved in the vertical direction, which

allows the sample to be irradiated at or away from the laser focal plane. This is essentially tuning the laser energy density in the treated region and will have an impact on the transferred metal lines. The laser scanning speed was adjusted not only to ensure enough overlapping of transferred metals for the continuity of electrodes but also to minimize the damage to the junction underneath the passivation layer. The laser scanning pattern on the front surface was controlled by the computer to produce a busbar with raster scanning and finger electrodes with single-pass scanning. The laser scanning pattern on the rear consisted of parallel lines with a spacing of 150 µm. Electro-plating of silver was performed to thicken the front laser-transferred titanium seed layer. About 2 to 3 µm thickness of silver was plated. An aluminum layer with thickness of 1 µm was evaporated on the rear side to complete the cell. The surface morphology of laser-transferred metal lines was investigated by a Zeiss SUPRA 40 scanning electron microscope (SEM). Contact resistivity of laser-transferred contacts (Si-Ti and Si-Al) was measured using the transmission line method (TLM). Solar cells based on All-Laser-Transferred Contacts were characterized in terms of J-V characteristics from which open-circuit voltage, short-circuit current, fill factor, series resistance and conversion efficiency were extracted.

2.3 Results and Discussion

2.3.1 Single laser pulse study and surface morphology

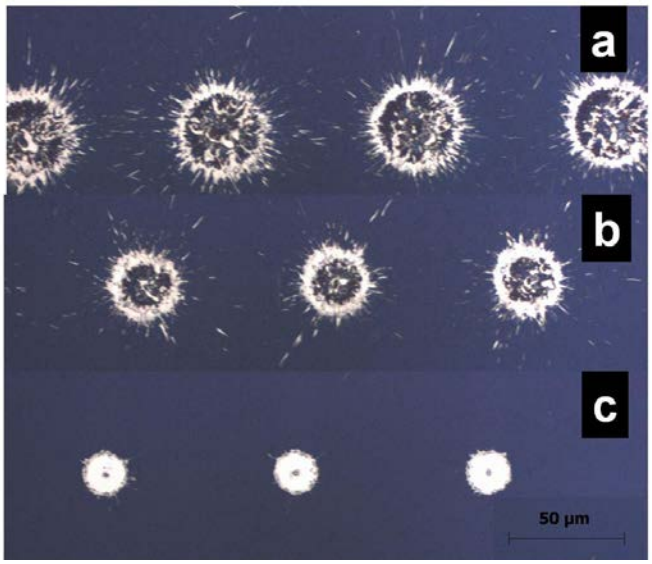

Figure 3. Optical microscope image of transferred metal spots created by single laser pulse with different energy densities: (a) 1.1 J/cm^2, (b) 0.90 J/cm^2 and (c) 0.69 J/cm^2.

Figure 3 shows the optical microscope images of laser-transferred spots each created by a single laser pulse along the scanning path. This is achieved by using a scanning speed high enough so that laser pulses do not overlap each other. The laser energy density is adjusted by tuning the energy per pulse on laser module. The focal position is fixed and spot size remains relatively constant. In this experiment, titanium is transferred to a silicon substrate coated with 70 nm thin layer of SiN_x. Laser pulses with energy density of 1.1 J/cm^2 transfer a larger area of Ti but ablate the center zone showing splashing patterns as seen in figures 3 (a). SEM images (not shown here) indicate peeling-off of SiN_x and a rough surface of melted silicon in the center. This laser energy density is not favored for metallization since transferred metals are not uniform and junctions underneath could be damaged. Laser pulses with a lower energy density of 0.90 J/cm^2 still causes splashing of the transferred Ti but results in less damage to the silicon substrate in the center. As laser power goes down to 0.69 J/cm^2, the transferred Ti forms

a more uniform coverage, and no splashing is observed (see figure 3 (c)). This observation at different laser energy density levels is consistent with the model given in reference [37]. Vaporization at the metal-glass interface pushes out the metal layer, either in the molten state or the partially molten state depending on the laser power, to realize the transferring. As seen from figure 3, the transferred Ti could be totally melted by laser pulses with higher power, and the vapor pressure is strong enough to ablate the molten Ti and a splashing pattern is observed. At lower power levels, the vapor pressure created by the laser beam transfers the Ti layer but with less intense force and results in a relatively uniform transferred spot as shown in figure 3(c).

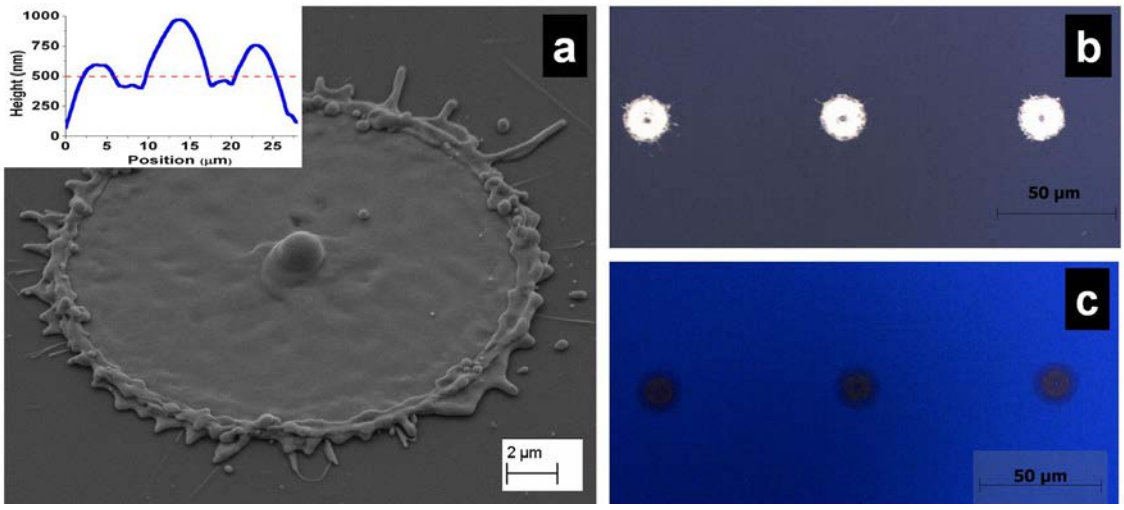

Figure 4. Laser-transferred Ti spot using a single laser pulse with energy density of 0.69 J/cm^2: (a) SEM image of a single spot; inset shows the profile with a dashed line indicating a height of 500 nm, (b) Optical microscope image of three single spots and (c) three single spots after etching back of Ti.

Further investigations for single laser pulse study are carried out and additional results are shown in figure 4. The SEM image in figure 4(a) is taken at a tilt angle of 45 degrees. A laser-transferred Ti spot is observed with surface roughness induced by laser

melting process. The original coating of Ti on glass had a thickness of 500 nm. However, the transferred spot has an uneven surface with a center protrusion and high ridges on the edge. The inset in figure 4(a) shows the profile with the dashed line indicating the thickness level of 500 nm. The ridges may be induced by a mild splashing process due to a shockwave [38] generated during laser transferring. The center protrusion could be the lifted silicon or expanded metal volume resulting from spinodal breakdown [38] due to the high laser energy density in the center resulting from the Gaussian laser beam profile. Figure 4(c) shows the image after etching back of Ti in the three transferred spots shown in figure 4(b). The etching is performed in a solution mixture of ammonium hydroxide and hydrogen peroxide for 2 minutes, which does not etch SiN_x. By comparison of figure 4(b) and 4(c), it can be seen that the laser-transferred Ti appears to have been fired through the SiN_x, and thus an ohmic contact to the emitter may be formed. However, further study through EDX or other characterization tools is needed to verify this.

2.3.2 Contact resistivity of front and rear laser-transferred metal contacts

Laser-transferred contact lines are formed when the laser scanning speed is decreased so that the laser pulses overlap. The scanning speed for the front Ti-Si contact is adjusted to have about 25% overlapping between laser spots while for rear Al-Si contact the overlapping is about 75% to ensure the possible formation of a back surface field. The first laser pulse transfers a Ti spot as shown in figure 3(c) and then the following overlapping laser pulses fire the as-transferred Ti through the SiN_x and SiO_2 dielectric layers and form the Ti-Si contacts. Contact resistivity of this laser-transferred Ti seed layer is measured using a testing structure as shown in the inset of figure 5. An n-

type emitter with a sheet resistance of 40 Ω/sq was fabricated on chemically textured p-type (ρ = 1~10 Ω-cm) silicon wafer followed by coating of passivation dielectric layers consisting of a stack of 15 nm SiO_2 and 60 nm SiN_x. The distance between the two laser-transferred Ti pads is kept at 200 µm and the length of each contact pad is 1 cm and the width is around 20 µm. The measurement setup is based on the principle of transmission line method (TLM) [39]. However, the emitter is highly doped to a level of 40 Ω/sq and thus the resistance between the two laser-transferred contact pads can be ignored in the calculation of the contact resistivity. Therefore, the contact resistivity can be calculated as the contact area multiplied by the inverse of the slope of the I-V curves in figure 5. Contact resistivity of laser-transferred Al-Si contacts is measured in a similar testing structure. The thickness of SiN_x is 120 nm.

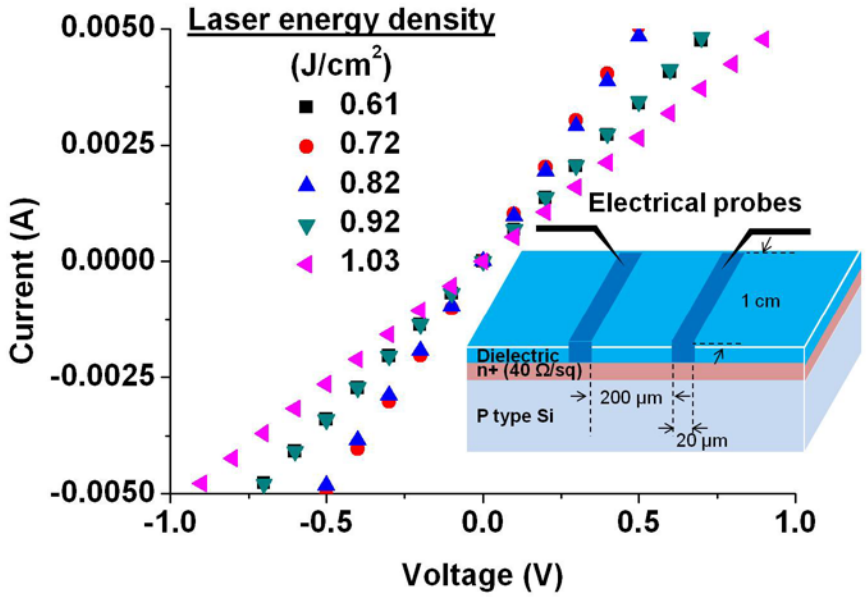

Figure 5. I-V curves for the laser-transferred Ti contacts at different laser energy densities; inset shows the testing structure and measurement setup.

As seen from figure 5, the I-V curves using the laser-transferred Ti-Si contacts are straight within the tested voltage range showing ohmic-contact characteristics. Similar curves were observed for laser-transferred Al-Si contacts but are not shown here. These experiments were carried out with the sample surfaces away from focal plane. This allows a relatively larger process window for the formation of laser-transferred contact lines. The laser transfer experiments started with an energy density of 0.61 J/cm^2 where the laser power is just enough to transfer the Ti layer and increased up to 1.03 J/cm^2 where laser power is ablating the transferred Ti layer as shown in figures 3(a) and 3(b). Compared to that at focal plane, the spot size was enlarged slightly to around 20 μm and it remained relatively constant at the laser energy densities used in this section.

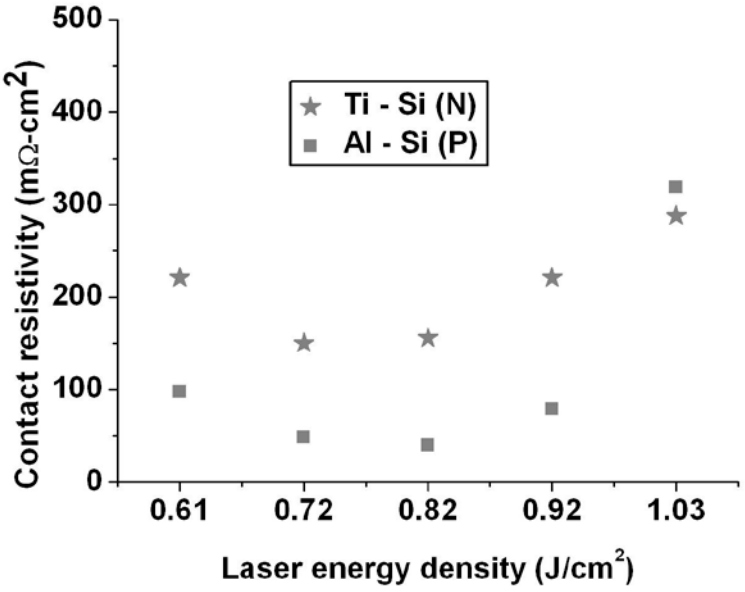

Figure 6. Contact resistivity of laser-transferred Ti-Si and Al-Si contacts at different laser energy densities.

The calculated contact resistivity based on the measurements is shown in figure 6. The contact resistivity decreased as the laser energy density was increased from 0.61 J/cm^2 to 0.82 J/cm^2. As laser power increases further, more transferred Ti is ablated and

the contact line becomes discontinuous at some regions resulting in less conductivity in the lateral direction. A similar trend was observed for laser-transferred Al-Si contacts. The contact resistivity shown in figure 6 for the laser-transferred Ti-Si seed layer is still relatively high. However, it decreases to around 25 mΩ-cm^2 after electro-plating of silver and further down to around 8 mΩ-cm^2 after a forming gas annealing for 2 minutes at 400 °C. It should be noted that the calculation of contact resistivity is based on the assumption that all the transferred metal is in ohmic contact with silicon. However, some part of the transferred metal could still lie on the dielectric layer and is not fired through to make an ohmic contact particularly at low laser energy density, as energy density may be low to penetrate the dielectric layer. Therefore, the contact area could be actually smaller and the values of calculations shown here should represent the maximum of contact resistivity for laser transferred contacts. This could be more significant for the calculations in the case of high laser energy densities which ablate the transferred metal. The actual contact area could be reduced by laser ablation. However, this laser ablation results in damage to the junction and forms discontinuous contact lines. A laser energy density of 0.72 J/cm^2 was chosen for the front-side metallization for the purpose of low contact resistivity with minimum damage to the junction. The same laser energy density was chosen for rear-side metallization but with more overlapping of laser pulses as discussed in the beginning of this section.

2.3.3 Solar cell performance with all-laser-transferred contacts

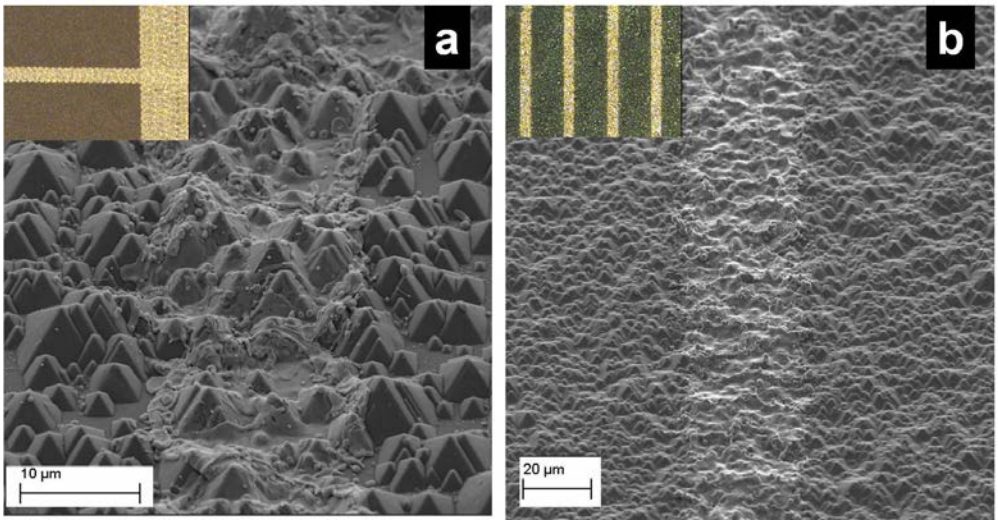

Figure 7. (a) Laser-transferred Ti contact (seed layer) on the front side; the inset shows an optical microscope image of a finger electrode connecting with a busbar (b) Laser transferred Al contact on the rear side; the inset shows an optical microscope image of parallel electrodes with dielectric in between. The width of front electrodes after plating is around 20 µm with a spacing of 400 µm. The width of the rear Al lines is around 30 µm with a spacing of 150 µm.

Silicon solar cells of 1 cm^2 square size were fabricated based on the ALTC process. The polished side of silicon wafer went through a chemical texturing using TMAH solution at 80℃ for 30 minutes while the other side, wire-saw cut with some roughness and damage, went through a damage etching step in KOH solution at 50℃ for 5 minutes and some roughness was left. Then the silicon wafer was processed as discussed in experimental section resulting in a passivated emitter with a stack of SiN_x/SiO_x (60 nm/15 nm) on the front surface and a passivated rear surface with a stack of SiO_x/SiN_x (5 nm/120 nm). Surface morphologies after laser-transferring metallization are shown in figure 7. As seen from figure 7(a), the laser-transferred Ti forms continuous finger electrodes and a busbar and coats well on the textured silicon surface. The final

width of these electrodes after electro-plating is around 20 μm, thinner than the reported value in [30]. The line width can be controlled by the laser power and the beam profile. As for the device in figure 7, laser energy density of 0.72 J/cm^2 was used for both transferring Ti and Al. The focal spot size was about 20 μm and the repetition rate of laser pulses was 20 kHz. The overlapping of laser pulses for transferring Ti was about 25% to minimize the damage to the junction while maintaining low contact conductivity. The busbar was formed by scanning laser beams in both x and y directions with same overlapping ratio of 25%. The overlapping of laser pulses for transferring Al is over 75% to ensure a deep back surface field. For comparison, a control device was fabricated on chemically textured silicon wafer, but the metallization was done using vacuum evaporation. Photolithography was performed to define the same front contact pattern as the ALTC cell and then the metal was deposited by e-beam evaporation. Rear contacts were achieved using full area aluminum paste fired at 800℃ for 5 minutes to form a back surface field. Fabrication details are mentioned in the experimental section and are not repeated here. The device performance parameters are shown in the following figure 8 and table 1.

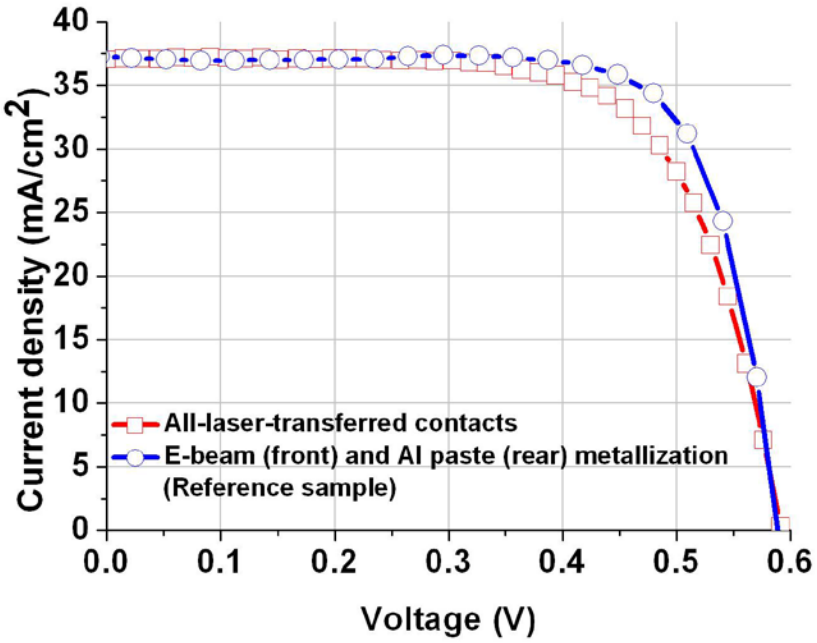

Figure 8. Illuminated I-V characteristics of an ALTC solar cell and a reference cell.

Table 1. Device parameter summary at 1-sun illumination.

Device parameters	All-Laser-Transferred Contacts	E-beam (front) and Al paste (rear) (Reference)
V_{oc} (mV)	592	590
J_{sc} (mA/cm^2)	37.1	37.2
Fill Factor (%)	69	75
Efficiency (%)	15.1	16.5
R_s (Ω)	1.9	0.7
R_p (Ω)	228	4348

The initial device in this study showed a conversion efficiency of 15.1%. The electrical parameters are extracted from figure 8 and are shown in table 1. By comparison, similar open-circuit voltages are achieved on both devices. Considering that similar fabrication conditions are used for junction formation and surface passivation, a back surface field should also form in the cell based on all-laser-transferred contacts. The

similar V_{oc} values for the ALTC cell and the control cell indicate that there is no significant degradation in the junction of the ALTC cell. However, the rear passivation on ALTC cell is not improving the V_{oc} over the control cell with full area Al-BSF. This could be due to the laser induced damage that results in recombination sites for the charge carriers. The extracted series resistance is larger for the ALTC cell than for the control cell and the shunt resistance is much smaller. This explains the relatively low fill factor of 69% of the ALTC cell, which is limiting the cell performance. To lower this series resistance, laser power, pulse overlapping and other experimental parameters need to be further optimized in future work.

2.3.4 PC1D simulation: Future improvements

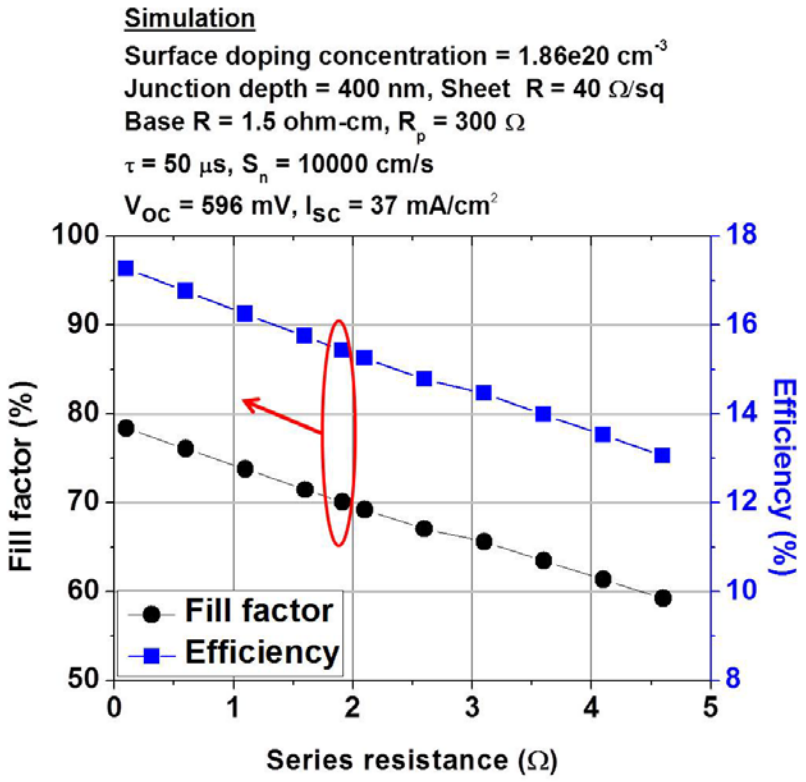

Figure 9. Simulated fill factor and efficiency as a function of series resistance using PC1D. The solid arrow is pointing at future improvements direction.

To demonstrate the future potential performance of solar cells based on All-Laser-Transferred Contacts, a simulation using PC1D was performed. The changes in fill factor and efficiency as a function of series resistance are plotted in figure 9. The parameters used in the simulation are shown above the figure. The doping recipe developed in our lab produces a high surface doping concentration with sheet resistance of around 40 Ω/sq and a junction depth of around 400 nm. Other parameters including bulk lifetime and surface recombination velocity are set to match the specifications of the wafer and the measured open-circuit voltage of 592 mV. The short-circuit current value is adjusted to match the measurement. It can be seen that the fill factor goes up to 76% and efficiency goes up to 17% as the series resistance is reduced to around 0.5 Ω which is achievable in

high efficiency reference solar cell. However, it should be noticed that the open-circuit voltage is relatively low in both the ALTC and control cells. This could be caused by the high surface doping concentration, low bulk quality of starting wafer and inadequate surface passivation limited by fabrication facilities. With improved open-circuit voltages, conversion efficiencies over 18% are expected showing the potential of all-laser-transferred contacts in high efficiency solar cell applications.

2.4 Summary

The fabrication process of All-Laser-Transferred Contacts is demonstrated for the first time on crystalline silicon wafers. The fabrication process is greatly simplified since a laser can transfer and fire various metals through dielectric passivation layers. Both the front and rear contacts have been laser-transferred indicating the great potential of lasers in simplifying the manufacturing of silicon solar cells. A single laser-pulse study was carried out to better understand this process. Silicon solar cells based on All-Laser-Transferred Contacts were fabricated, achieving an initial conversion efficiency of 15.1%. Further improvements are expected in the efficiency by increasing the open-circuit voltage and reducing the series resistance through optimization of the laser transfer and the fabrication processes.

CHAPTER 3: LASER TRASNFER OF DOPANTS

3.1 Introduction

In this chapter, we investigate the application of laser transfer of dopants. Traditional furnace diffusion for emitter is a process that requires high temperature. The laser transferring process is capable of locally driving in the dopants to form localized emitter on silicon. Furthermore, this is a room-temperature process without thermal effect on the bulk silicon.

In this chapter, the laser transferring process of dopants is demonstrated and combined with laser transfer of contacts to achieve an all laser transfer process for fabricating silicon solar cells. The front-side p-n junction was formed by a laser transferring phosphorus doped glass and a-Si layers. Electro-plating was used to successfully deposit metal on the laser-transferred line-shaped junctions. The rear side was metallized by locally laser transferring Al through the passivation dielectric layer as demonstrated in the previous chapter. This initial work of the All-Laser-Transfer process at room temperature demonstrates the concept of all laser-based processing for silicon solar cell fabrication.

3.2 Experimental

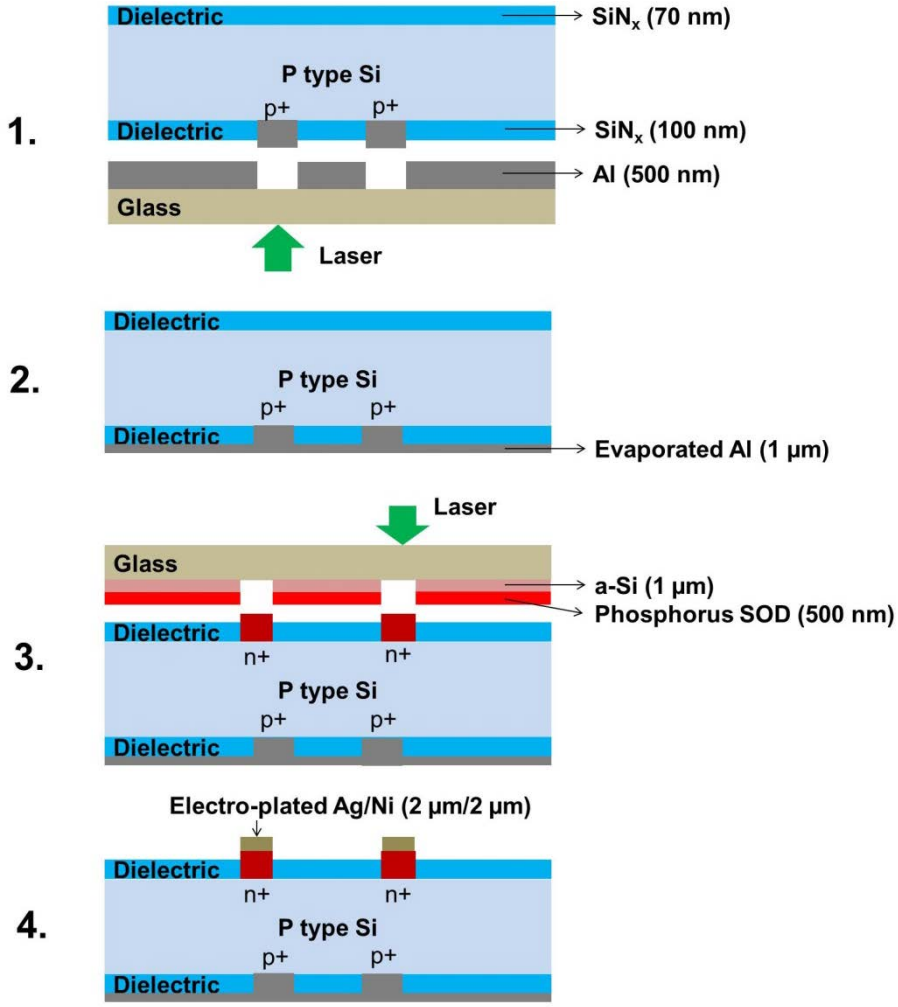

Figure 10. Schematic of fabrication steps of All-Room-Temperature and All-Laser-Transferred process for silicon solar cell. Step 1 and 2 shows the transfer of back metal contact and rear side metallization, step 3 shows transfer of dopant layer and step 4 shows final electroplating process.

The fabrication process is shown in figure 10, indicating four major steps. P-type boron-doped silicon wafers (Fz) with resistivity of about 1 Ω-cm, thickness of 280 µm and crystalline orientation of <100> were used in the experiments. The wafers were first cleaned for the removal of organic and metallic contaminants in Piranha solution at 85℃

for 10 minutes. In this initial work no surface texturing was performed. A SiN_x layer of 70 nm was deposited by PECVD on the front side to serve as both an antireflection and a passivation layer. Another SiN_x layer of 100 nm was deposited on the rear side for passivation. These two layers of SiN_x are labeled as the 'Dielectric' layer in figure 10.

The laser used for this laser transferring process is the same one as in the last chapter. The laser transfer of aluminum of 500 nm through the rear passivation SiN_x layer was carried out to form base contacts. The contact lines have width of about 15 μm with spacing of about 250 μm. An aluminum layer of about 1 μm thickness is then evaporated on the rear side in step 2.

In step 3, another glass slide was coated with a dopant stack which included an amorphous silicon layer of 1 μm deposited by PECVD and a phosphorous spin-on dopant (Filmtronics P509) layer of about 500 nm. Then the glass slide with coating is brought in contact with the front side of Si wafer and laser transferring was performed. The line-shaped junctions have width of about 15 μm with spacing of about 200 μm. The amorphous silicon layer serves as the carrier of the spin-on dopants (SOD) to be transferred since amorphous silicon absorbs laser energy at 532 nm much more effectively than transparent soft baked SOD layer. It should be noted that dopants stack could be replaced with a single layer of doped amorphous silicon layer such as a-Si:P for simplification. Electro-plating of Ag/Ni (2 μm/2 μm) was performed in step 4 for metallization. Therefore, only four steps were performed to finish the cell fabrication starting with a p-type dielectric-coated silicon wafer. Furthermore, the processing is performed at room temperature, which eliminates the detrimental effects of wafer contamination from high temperature processing.

3.3 Results and Discussion

3.3.1 Junction geometry

In contrast with the traditional full-area junction, localized line-shaped junctions were formed by laser transfer doping process. The junction geometry plays a significant role in determining the final cell performance. More specifically, the junction geometry in this work is defined by the laser scanning pattern. The front junction (grid) pattern for fabricated cells was connected to a bus bar in the center and finger electrodes were perpendicular. The spacing d between the line-shaped junctions was optimized.

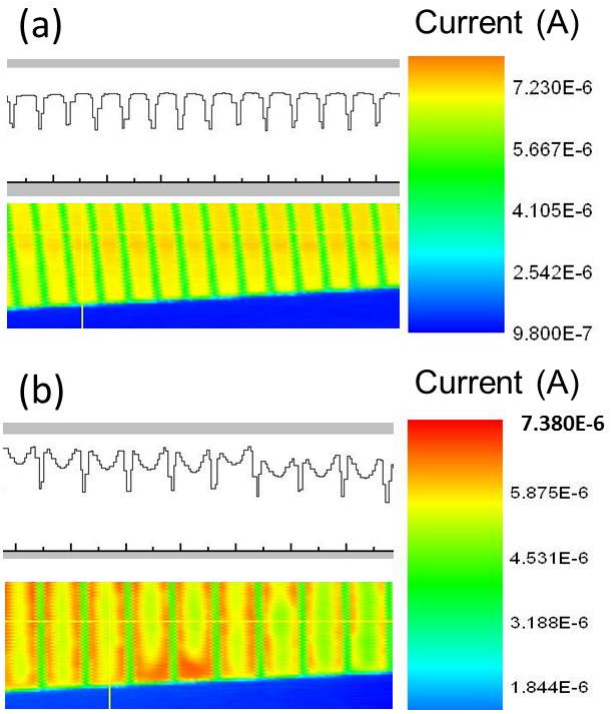

Figure 11. Current mapping data for cells with localized line-shaped junctions formed by laser transfer doping process. (a) Junction spacing d = 200 µm, (b) d = 300 µm. The top part in each figure shows the scanning profile of current magnitudes across the fingers

and the lower part shows the current mapping (resolution = 20 μm) with color codes on side.

As seen from the scanning profiles of current in figure 11, the current distribution is more uniform with a finger spacing of 200 μm, showing the carriers travelling to the localized junctions under the metal contacts. Therefore, the finger electrodes with spacing of 200 μm effectively collected the photo-generated carriers and this geometry is chosen for the initial device.

3.3.2 Optical images

During the laser transfer doping process, the laser transfers the dopants to the silicon wafer and fires through the dielectric layer. This results in the local melting of silicon which accelerates the diffusion of dopants.

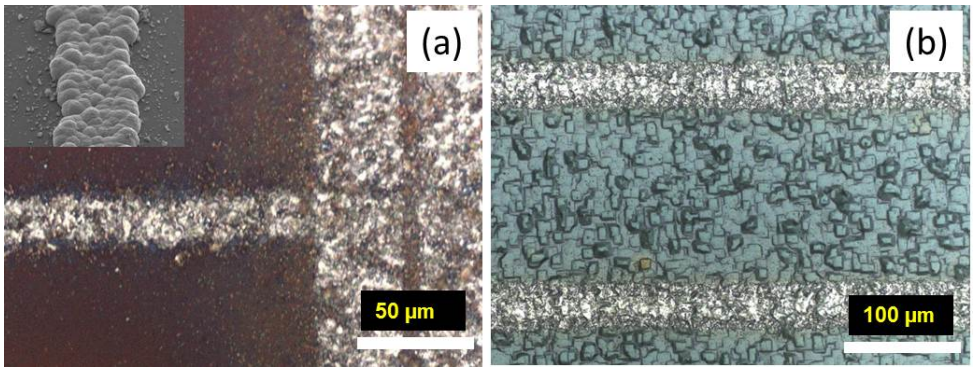

Figure 12. (a) Optical microscope image of laser transferred junction showing a finger perpendicular to bus bar before electro-plating. The inset is the SEM image of the laser transferred junction after Ni plating. (b) Optical microscope image of laser transferred back Al contact lines.

As seen from figure 12(a), the laser transferred region shows a different contrast as a result of opening of dielectrics and the roughness induced from local melting of silicon. The inset of figure 12(a) shows successful plating of nickel on laser-transferred doped lines indicating the effective activation of dopants by laser transferring process. Figure 12(b) shows the optical microscope image of laser transferred aluminum lines contacting the base. The roughness in the shape of square pits across the area resulted from the damage etching of initial as-cut wafer.

3.3.3 Cell performance

The initial device fabricated in the All-Room-Temperature and All-Laser-Transfer process showed short circuit current density as high as 34.5 mA/cm^2. The open-circuit voltage and fill factor of the initial non-optimized device are 328 mV and 36% respectively. The low V_{oc} could be a result of non-optimized laser condition such as laser pulse energy density, number of overlapping pulses, etc. More work need be done to optimize these parameters.

The low V_{oc} may also be due to parasitic shunting at the rear contacts due to an inversion layer created by the fixed positive charge in the SiN_x [40]. While an inversion layer at the front contact induced by the SiN_x antireflection layer may assist in the collection of minority carriers, an inversion layer at the rear surface may cause increased recombination at the laser-transferred Al contact lines. This type of parasitic shunting can be prevented by using an Al_2O_3 passivation layer on the rear surface since the fixed negative charge in the Al_2O_3 will generate an accumulation layer in the p-type Si [41].

From I-V measurement, the calculated series resistance was 5 Ω, significantly affecting the fill factor. It should be pointed out that the initial device with electro-plated Ni did not go through a low temperature (~300℃) annealing/firing process which could improve the nickel-silicon contacts significantly. Despite the low values of V_{oc} and FF, the external quantum efficiency is comparable with those of reported solar cells as shown in figure 13. However, long wavelength response needs to be improved further.

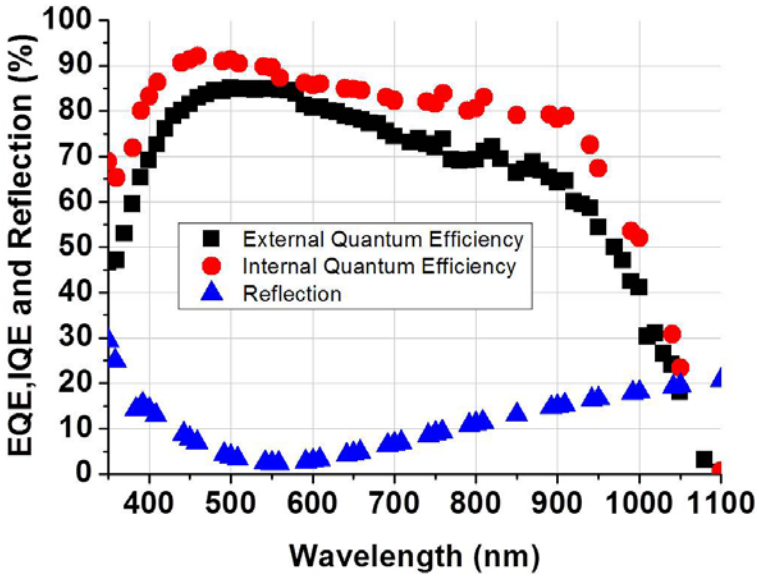

Figure 13. Quantum efficiencies and optical reflection of a silicon solar cell fabricated by All-Laser-Transferred process at room temperature.

The EQE value over the short wave-length spectrum indicates an effective carrier separation efficiency by the laser transferred localized junction. However, EQE decreases after 550 nm wavelength and this might be due to recombination at the rear surface Al contact lines as a result of the induced inversion layer. More characterization work needs to be carried out to investigate the possible degradation of carrier lifetime in laser transfer process.

3.3.4 PC2D Simulation: Potential of All-Laser-Transfer solar cell

To study the effects of two dimensional device structure based on All-Laser-Transfer process, a PC2D simulation was performed [42]. The cell structure parameters used in the simulation were line junction width of 20 μm and junction spacing of 200 μm. Without a detailed investigation of the laser doping profile, the junction sheet resistance was assumed to be 20 Ω/sq to represent the relatively high doping level by laser transfer process. The carrier lifetime value was set as 100 μs. The surface recombination current for un-doped surface region was set as 50 fA/cm^2, which is obtainable for a well passivated P type surface. This assumed low level of surface recombination current, an advantage for the all-laser-transferred cell since the majority of the surface area is not affected by doping. The calculated parameters are shown in table 2.

Table 2. Simulated electrical parameters by PC2D.

J_{sc} (mA/cm^2)	V_{oc} (mV)	Efficiency (%)
34.3	660	18.4

R_s = 0.8 Ω, R_p = 10 kΩ; τ = 1 ms; Sheet R (laser transfer doped) = 20 Ω/sq.

As seen from the table above, with a well passivated surface and optimized laser transferring conditions, the silicon solar cell has the potential of reaching a conversion efficiency of 18.4%. The introduction of surface texturing in future all-laser-transferred cells is expected to bring up the short-circuit current and hence calculated overall efficiency to over 20%. More work needs to be carried out to improve the open-circuit voltage, fill factor and understanding the loss mechanisms as well as theoretical limit of short-circuit current.

3.4 Summary

An All-Room-Temperature and All-Laser-Transfer silicon solar cell fabrication process is demonstrated. It eliminates the high-temperature process and shows the potential of All-Laser-Based process in lowering the fabrication cost. Despite of the low conversion efficiency obtained from the initial device, high current density level of 34.5 mA/cm^2 and reasonable EQE indicates the future potential of this simple and low-cost process. Future work needs to be focused on optimizing the laser conditions and modifying the rear surface passivation layer to improve V_{oc} and inserting an annealing step to lower the contact resistance and hence improvement in the fill factor.

CHAPTER 4: CONCLUSION AND FUTURE WORK

4.1 Conclusion

The laser transferring process of metal contacts and dopants have been studied. The experimental conditions were described to demonstrate the application of laser transferring for metallization and doping for fabricating silicon solar cells. Optical and electrical characterizations were performed to understand the effect of laser transferring process on materials properties. Devices were fabricated using laser transferred contacts and dopants. Based on these findings, the conclusions of this research are drawn as follows:

1. Both titanium and aluminum of about 500 nm in thickness were successfully laser transferred from glass slides to silicon wafer and ohmic contacts were formed. Contact resistivity as low as 8 mΩ-cm^2 was achieved for laser transferred Ti on highly doped silicon emitter (surface doping concentration ~ 3e20/cm^3) after electro-plating and low temperature firing at 400℃. Contact resistivity of about 50 mΩ-cm^2 was achieved for laser transferred Al on lightly doped P type silicon.

2. Microscope and SEM images show that uniform Ti spots were transferred with single laser pulses. Overlapping laser pulses transferred the metal and formed continuous lines to conduct current.

3. Silicon solar cells based on ALTC were fabricated achieving an initial conversion efficiency of 15.1%.

4. The phosphorus dopant was successfully laser transferred through the dielectric passivation and antireflection layer. The details of the experimental conditions and

sequence were discussed. The obtained efficiency of 4.1% was low but further optimization of laser transfer and fabrication process should improve it further.

5. In combination with laser transferred contacts, the laser transfer doping process was applied for fabricating silicon solar cells at room temperature by an all-laser-transfer process. The fabricated cell features a line-shape localized junction metallized by electro-plating. The rear contacts were laser transferred. The initial solar cell fabricated by this all-laser-transfer process showed short circuit current of 34.5 mA/cm^2 with carrier collection confirmed by LBIC.

4.2 Future Work

1. The pulse duration of the laser used for this work is 1 ns. It would be interesting to investigate into the effect of longer pulse duration on the performance of laser transferring of metal contacts and dopants. Longer pulse duration in a certain range might facilitate the diffusion of the metal or dopants and therefore potentially improve the device results.

2. The metal and dopants have been laser transferred through 70 nm dielectric layers of SiN_x. It would be interesting to research in the effects of dielectric layers on the performance of laser transferring process. Different materials of dielectric layers or difference thickness might play a vital role in the resultant contact resistivity of laser transferred contacts.

3. The carrier of laser transferred films is a transparent glass slide in this work, and the laser transferring process has been performed in air. More materials characterization could be carried out to investigate and confirm the composition. The

oxidation of laser transferred metal or incorporation of glass could degrade the conductivity of the laser transferred contacts.

4. It would also be interesting to apply the laser transferring process of metal contacts and dopants for advanced silicon solar cell structures. Both positive and negative contacts for Interdigitated Back Contacts (IBC) could be achieved with laser transferring process. Laser transfer doping could also be potentially applicable for selective emitters in advanced solar cells.

CHAPTER 5: OTHER RESEARCH

Integration of Solar Cell and Module-level Contacts by Laser Welding of Al Foil

5.1 Introduction

Traditional fabrication process of silicon solar cells based on full-area Al-BSF generally requires printing of another Ag pad on the Al-printed rear side in order to solder copper ribbon. This requires additional step and increases the cost since metallization paste make up the largest portion of current process costs besides wafer materials [43]. Aluminum foil is a very cost-effective source of metallization material for silicon solar cells. On cell level metallization, aluminum foil has been laser fired through rear passivation dielectric layer and into silicon to form the contacts similarly to laser fired contact (LFC) [44]. To flatten the Al foil surface for laser processing, it was applied on a vacuum stage. The aluminum foil was then left on the cell after laser processing. On module level metallization, aluminum foil has been stacked with silicone encapsulant for laser welding for the interconnection of back contacts [45]. High resistance to mechanical stress and low electrical contact resistance were achieved on the modules based on this laser welding process.

In this work, silicon solar cell and module-level contacts were achieved by laser processing of 8 μm thick aluminum foil. A stack of glass and aluminum foil was brought in contact with the rear side of silicon wafer coated with passivation dielectric layer. The pulsed 1064 nm laser then fired the aluminum foil into silicon to form an ohmic contact and at the same time welded the silicon wafer, aluminum foil and glass substrate together to mechanically assemble the module. Cross-section morphology and composition of laser fired contacts at different laser processing conditions were studied and contact

resistivity of rear contacts was characterized. Initial cell welded to glass substrate through Al foil showed conversion efficiency of 15.9%. A simulation was performed to investigate the effect of increased rear internal reflection on short circuit current as an advantage of this process. As a proof-of-concept, this work utilized the low-cost aluminum foil and laser processing to integrate the back cell and module-level contacts and demonstrated the potential of this technique on simplifying cell and module fabrication in a cost-effective way.

5.2 Experimental

Fabrication process sequence for surface texturing, emitter diffusion and passivation of both sides followed the process as described in chapter 1 and will not be repeated here. Rear side contact formation process was based on laser welding of aluminum foil by passing laser beam through a glass substrate which ultimately realizes the concept of integrating cell and module-level contacts. The aluminum foil used in this work has a thickness of 8 μm. As a result of the low stiffness, the Al foil could have wrinkles on surface which could interfere with laser processing. Therefore, it is important to flatten the foil for the laser processing. Instead of using any vacuum system or adhesive materials, a soda lime glass (thickness = 1.2 mm, softening temperature = 720℃) was placed upon Al foil on top of the silicon wafer as shown in figure 14. The pressure from glass substrate is proven to be enough for flattening the foil and uniform laser processing occurs throughout the sample area. Furthermore, the glass substrate was welded to Al foil. As a back substrate of the as-fabricated solar cell, the glass remains on

the rear side, and with further interconnection and EVA lamination the final module could be realized.

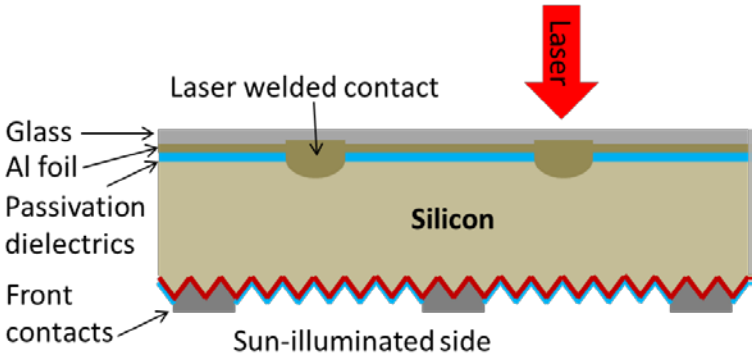

Figure 14. Schematic of laser welding process for Al foil to rear side of silicon solar cell.

A Q-switched pulsed Ytterbium fiber laser, with wavelength of 1064 nm and pulse duration of 50 ns, was used for this work. The energy per pulse at maximum output is 1 mJ/pulse. The laser beam was passed through a convex lens to focus on the surface of Al foil with an effective focal spot size of about 50 µm. Throughout the process, the laser beam was stationary but the samples were moved on a computer controlled xy stage. Laser output power and stage speed were varied to study their effects on the contacts formation and the results are reported in the following sections. The stage speed was used to calculate the number of overlapping pulses at a given spot.

5.3 Results and Discussion

5.3.1 Morphology study

In order to investigate the cross section morphology, test silicon samples after laser processing were peeled off from the glass substrate with Al foil and then cleaved.

The sample in the following figure was processed with laser energy density of E = 6.5 J/cm^2 and number of laser pulses at a given spot N = 130.

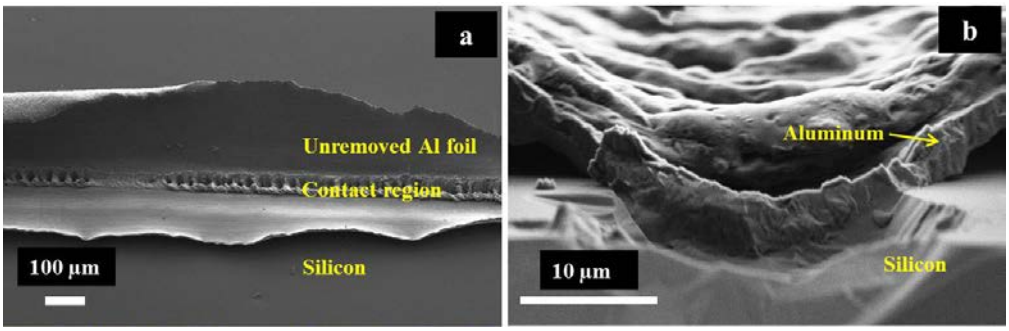

Figure 15. SEM images of laser welded Al foil on silicon wafer with E = 6.5 J/cm^2 and N = 130. (a) Titled view at 45 degrees; (b) Cross section of (a).

As shown in figure 15, significant roughness was generated in the laser welding trench. The laser welding region depth was as shallow as about 3 µm. A distinct transition from aluminum to silicon was observed and hence Si-Al could be formed. This was also confirmed by EDX data which is not shown here. Electrical contact resistivity of about 1.8 mΩ-cm^2 was achieved.

5.3.2 Device performance

Laser processing condition in figure 15 was chosen for laser welding of Al foil to silicon and glass substrate to fabricate the initial silicon solar cell device. The device results are plotted and summarized in figure 16 with an inset picture of the rear side of the real device welded to glass.

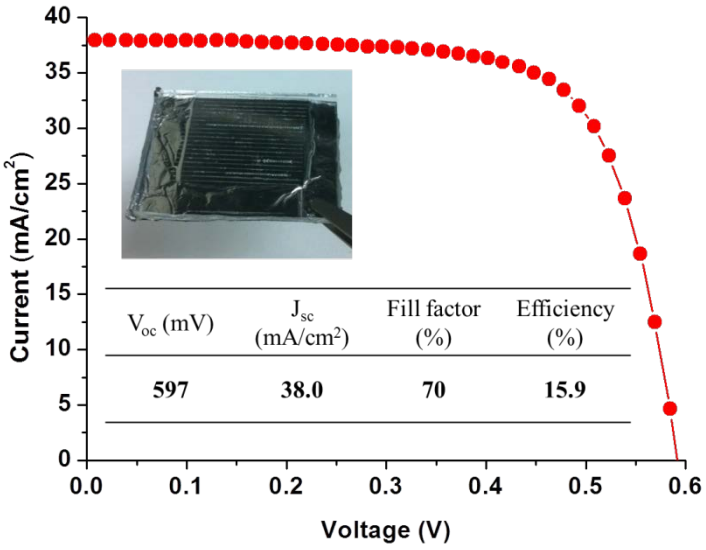

Figure 16. Illuminated J-V characteristics of Al foil based laser welded silicon solar cell on glass: Device results are summarized in the inset table and the inset picture shows the rear side of the actual device.

As shown in the inset of figure 16, the rear side of the as-fabricated silicon solar cell was mechanically welded with the Al foil to glass substrate. The wrinkles around device resulted from the handling process. The active area of the Al foil on device remained relatively flat and was bonded with the glass through laser welding lines. After a forming gas (95% Ar, 5% H_2) annealing for two minutes at 400℃, the device was characterized using the 1-sun simulator and the electrical parameters were extracted from the illuminated J-V curve and summarized in the inset table of figure 16. The implied V_{oc} of the silicon wafer measured by Sinton Suns-V_{oc} before metallization was about 637 mV, indicating further improvements are desired through optimization of laser process. The initial efficiency was 15.9% with a high short circuit current of 38.0 mA/cm^2. Compared to the average J_{sc} value of about 36.3 mA/cm^2 of our reference baseline cells, the short

circuit current increased by almost 2 mA/cm^2. However, it is noted that the fill factor of the final device is only about 70%. The device is affected by a high series resistance which could result from the nonuniform contact formation across the sample. Future work needs to be carried out to optimize the device fabrication process.

5.4 Summary

A laser welding process of silicon solar cell to glass using 8 μm thick Al foil was demonstrated. The demonstrated fabrication process for solar module could avoid the cost of Ag pad printing and tabbing. Moreover, the Si solar cell back contacts and module-level contacts were integrated in a single step using laser welding of Al foil to glass. Morphology studies were carried out using SEM on the interface of laser welded Al foil to silicon. The electrical contact resistivity as low as 1.8 mΩ-cm^2 was achieved. As a proof-of-concept, initial silicon solar cell bonded to glass showed conversion efficiency of 15.9%, which can be further improved. Future work needs to be carried out on the optimization of device performance.

PUBLICATIONS AND PRESENTATIONS

Longteng Wang, David E. Carlson and Mool C. Gupta, "Silicon Solar Cells Based on All-Laser-Transferred Contacts", *Progress in Photovoltaics: Research and Applications*, 2013, DOI: 10.1002/pip.2395.

Longteng Wang, David E. Carlson and Mool C. Gupta, "All-Laser-Transfer Process for Silicon Solar Cells", *IEEE 39th Photovoltaic Specialist conference proceedings*, Tampa, FL, 2013

Longteng Wang, David E. Carlson and Mool C. Gupta, "Investigation of metal contacts for silicon solar cells using laser processed 8 μm thick Al foils", *SPIE Optics+Photonics: Laser Materials Processing for Solar Energy Devices II*, 2013

Mool C. Gupta, ***Longteng Wang***, Christian Rothenbach and Keye Sun, "Diode Pumped Solid State Lasers for Surface Microtexture", *Journal of Laser Micro/Nanoengineering* 2013; 8(2): 124-130.

Longteng Wang, Vikram V. Iyengar and Mool C. Gupta, "Electric-arc micro-texturing of silicon surfaces for photovoltaic applications", *IEEE 38th Photovoltaic Specialist conference proceedings*, Austin, TX, 2012.

Mool C. Gupta, Barada Nayak, Vikram Iyengar and ***Longteng Wang***, "Efficient light trapping by laser microtexturing of surfaces for photovoltaics", *SPIE Newsroom*, 2012.

REFERENCES

[1] Saga T, Advances in crystalline silicon solar cell technology for industrial mass production. NPG Asia Materials 2010; 2(3): 96–102.
[2] Neuhaus DH, Munzer A, Industrial silicon wafer solar cells, Advances in Optoelectronics 2007; 2007: 24521, DOI: 10.1155/2007/24521.
[3] Sopori B, Mehta V, Rupnowski P, Moutinho H, Shaikh A, Khadilkar C, Bennett M, Carlson D, Studies on Backside Al-Contact Formation in Si Solar Cells: Fundamental Mechanisms. The proceedings of MRS Fall Meeting 2008; 1123: P07-11.
[4] Lin C, Tsai S, Hsu S, Hsieh M, Structural properties of the solidified-Al/regrown-Si structures of printed Al contacts on crystalline Si solar cells, Solar Energy Materials and Solar Cells 2008; 92: 986.
[5] Nijs JF, Szlufcik J, Poortmans J, Sivoththaman S, Mertens RP, Advanced manufacturing concepts for crystalline silicon solar cells, IEEE Transactions on Electron Devices 1999; 46: 1948.
[6] Mette A, New concepts for front side metallization of industrial silicon solar cells, PhD dissertation, Fraunhofer-Institut für Solare Energiesysteme, 2007, pp. 32- 36.
[7] Kaminski A, Vandelle B, Fave A, Boyeaux JP, Nam LQ, Monna R, Sarti D, Laugier A, Aluminum BSF in silicon solar cells, Solar Energy Materials and Solar Cells 2002; 72: 373.
[8] Narasimha S, Rohatgi A, Weeber AW, An optimized rapid aluminum back surface field technique for silicon solar cells, IEEE Transactions on Electron Devices 1999; 46: 1363.
[9] Hilali MM, Rohatgi A, To B, A review and understanding of screen-printed contacts and selective–emitter formation, 14th Workshop on Crystalline Silicon Solar Cells and Modules 2004.
[10] Lennon A, Yao Y, Wenham S, Evolution of metal plating for silicon solar cell metallization, Progress in Photovoltaics: Research and Applications 2012; doi: 10.1002/pip.2221.
[11] Kim DS, Lee EJ, Kim J, Lee SH, Low-cost contact formation of high-efficiency crystalline silicon solar cells by plating, Journal of the Korean Physical Society 2005; 46(5): 1208.
[12] Glunz SW, Rein S, Lee JY, Warta W, Minority carrier lifetime degradation in boron-doped Czochralski silicon. Journal of Applied Physics 2001; 90(5): 2397.
[13] Iyengar VV, Nayak BK, Gupta MC, Silicon PV devices based on a single step for doping, anti-reflection and surface passivation. Solar Energy Materials and Solar Cells 2010; 94: 2205.
[14] Shah PL, Fuller CR, Process for fabricating inexpensive high performance solar cells using doped oxide junction and insitu anti-reflection coatings, US Patent 4101351,1978.
[15] Grohe A, Knorz A, Nekarda J, Jäger U, Mingirulli N, Preu R, Novel laser technologies for crystalline silicon solar cell production. Invited paper- Proceedings of SPIE, Laser-based Micro- and Nanopackaging and Assembly III, 2009; 7202: 72020P, DOI: 10.1117/12.810128.
[16] Grohe A, Preu R, Glunz SW, Willeke G, Laser applications in crystalline silicon solar cell production. Proceedings of SPIE, Photonics for Solar Energy Systems, 2006; 6197: 619717, DOI: 10.1117/12.663225.

[17] Carlson DE, Laser processing for solar cells. Keynote paper- Proceedings of SPIE, Laser Material Processing for Solar Energy, 2012; 8473: 847302, DOI: 10.1117/12.932276.
[18] Nayak BK, Iyengar VV, Gupta MC, Efficient light trapping in silicon solar cells by ultrafast-laser-induced self-assembled micro/nano structures. Progress in Photovoltaics: Research and Applications 2011; 19: 631.
[19] Glunz, SW, Rein S, Warta W, Knobloch J, Wettling W, Degradation of carrier lifetime in Cz silicon solar cells. Solar Energy Materials and Solar Cells 2001; 65: 219.
[20] Schneiderlöchner E, Preu R, Ludermann R, Glunz SW, Laser fired rear contacts for crystalline silicon solar cells. Progress in Photovoltaics: Research and Applications 2002; 10: 29.
[21] Alemán M, Streek A, Regenfuß P, Mette A, Ebert R, Exner H, Glunz SW, Willeke G, Laser micro-sintering as a new metallization technique for silicon solar cells. Proceedings of 21st European Photovoltaic Solar Energy Conference, 2006; 705.
[22] Dube CE, Gonsiorawski RC, Improved contact metallization for high efficiency EFG polycrystalline silicon solar cells. Proceedings of 21st Photovoltaic Specialists Conference, 1990; 1: 624.
[23] Knorz A, Peters M, Grohe A, Harmel C, Preu R, Selective laser ablation of SiN_x layers on textured surfaces for low temperature front side metallizations. Progress in Photovoltaics: Research and Applications 2009; 17(2): 127-136.
[24] Mason NB, Bruton TM, Balbuena MA, PV in Europe – From PV Technology to Energy Solutions 2002; 227.
[25] Braudy RS, Laser writing. Proceedings of the IEEE, 1969; 57: 1771.
[26] Bohandy J, Kim BF, Adrian FJ, Metal deposition from a supported metal film using an excimer laser. Journal of Applied Physics 1986; 60: 1538
[27] Schultze V, Laser-induced forward transfer of aluminum. Applied Surface Science 1991; 52: 303.
[28] Kántor Z, Tóth Z, Szörényi T, Tóth AL, Deposition of micrometer sized tungsten patterns by laser transfer technique. Applied Physics Letter 1994; 64: 3506.
[29] Kantor Z, Toth Z, Szorenyi T, Laser induced Forward Transfer: the effect of support-film interface and film-to-substrate distance on transfer. Applied Physics A 1992; 54: 170.
[30] Röder TC, Hoffmann E, Köhler JR, Werner JH, 30 µm wide contacts on silicon cells by laser transfer. Proceedings of the 35th IEEE Photovoltaic Specialists Conference 2010; 003597
[31] Röder TC, Hoffmann E, Konrad B, Kohler JR, Low temperature laser metallization for silicon solar cells. Energy Procedia 2011; 8: 552.
[32] Blakers AW, Wang A, Milne AM, Zhao J, Green MA, 22.8% efficient silicon solar cell. Applied Physics Letters 1989; 55: 1363.
[33] Papet P, Nichiporuk O, Kaminski A, Rozier Y, Kraiem J, Lelievre JF, Chaumartin A, Fave A, Lemiti M, Pyramidal texturing of silicon solar cell with TMAH chemical anisotropic etching. Solar Energy Materials and Solar Cells 2006; 90: 2319.
[34] Iyengar VV, Nayak BK, Gupta MC, Silicon PV devices based on a single step for doping, anti-reflection and surface passivation. Solar Energy Materials and Solar Cells 2010; 94: 2205.

[35] Schmidt J, Kerr M, Cuevas A, Surface passivation of silicon solar cells using plasma-enhanced chemical-vapour-deposited SiN films and thin thermal SiO_2/plasma SiN stacks. Semiconductor Science and Technology 2001; 16: 164.
[36] Dullweber T, Gatz S, Hannebauer H, Falcon T, Hesse R, Schmidt J, Brendel R, 19.4%-efficient large area rear-passivated screen-printed silicon solar cells. Proceedings of 26th European Photovoltaic Solar Energy Conference 2011; 811.
[37] Röder TC, Köhler JR, Physical model for the laser induced forward transfer process. Applied Physics Letters 2012; 100: 071603.
[38] Bleiner D, Bogaerts A, Multiplicity and contiguity of ablation mechanisms in laser-assisted analytical micro-sampling. Spectrochimica Acta Part B 2006; 61: 421.
[39] http://www.cleanroom.byu.edu/contact_resistance.phtml, visited on October 31, 2012.
[40] I. Cesar, E. Bende, G. Galbiati, L. Janßen, A. A. Mewe1, P. Manshanden, A .W. Weeber, J.H. Bultman, Parasitic shunt losses in all-side SiN_x passivated mc-Si solar cells, 24th European Photovoltaic Solar Energy Conference 2009.
[41] B. Hoex, J. Schmidt, M. van de Sanden, W. Kessels, Crystalline silicon surface passivation by the negative-charge-dielectric Al_2O_3. IEEE 33rd Photovoltaic Specialist Conference 2008.
[42] P. Basore, K. Cabanas-Holmen, PC2D: A circular-reference spreadsheet solar cell device simulator. IEEE Journal of Photovoltaics 2011; 1: 72-77.
[43] International Technology Roadmap for Photovoltaics, 4th Ed., SEMI PV Group March 2013.
[44] J. Nekarda, M. Graf, A. Rodofili, A. Wolf, R. Preu, Proceedings of SPIE- Laser Material Processing for Solar Energy 2012; 8473: 847307.
[45] H. Schulte-Huxel, S. Blankemeyer, R. Bock, A. Merkle, S. Kajari-Schroder, R. Brendel, Al-foil on encapsulant for the Interconnection of Al-metalized silicon solar cells, IEEE Journal of Photovoltaics 2013; 3: 77- 82.